JMEPEG (2024) 33:10726–10735
https://doi.org/10.1007/s11665-023-08723-6

1059-9495/$19.00

ORIGINAL RESEARCH ARTICLE

Effect of High-Current Pulsed Electron Beam Irradiation on the Microstructure and Mechanical Properties of Multilayered TiN/TiCN/Al_2O_3 Coatings

Nana Tian, Shiyu Zhou, Conglin Zhang, Fuyang Cao, Jintong Guan, Xiangming Chen, and Qingfeng Guan

Submitted: 11 July 2023 / Revised: 16 August 2023 / Accepted: 31 August 2023 / Published online: 20 September 2023

This work investigates the effects of high-current pulsed electron beam (HCPEB) irradiation on multilayered TiN/TiCN/Al_2O_3 coatings deposited via chemical vapor deposition onto cemented carbide substrates. The study focuses on analyzing the impact of irradiation pulses on the phase composition, microstructure, mechanical properties, and cutting performance of these coatings. The results demonstrate that the multilayered TiN/TiCN/Al_2O_3 coatings exhibit a smooth surface with enhanced mechanical performance after HCPEB irradiation. Notably, the coating irradiated with 5 pulses achieves a maximum hardness of approximately 28.48 GPa, displaying improved wear resistance and cutting performance. These improvements can be primarily attributed to the enhancements in hardness and elastic modulus, along with the generation of residual compressive stress in the 5-pulse irradiated coating.

Keywords cutting performance, high-current pulsed electron beam,, nano-hardness, TiN/TiCN/Al_2O_3-coated carbide tool, wear performance

1. Introduction

High-performance cutting tools are highly required in the manufacturing industry (Ref 1). For decades, tungsten cobalt cemented carbide (WC-Co) tools have been widely used in machining difficult-to-cut materials due to their low thermal expansion coefficient, high hardness, and high elastic modulus (Ref 2). It is well known that cutting tools operate under extremely high loads and undergo severe abrasive wear during working conditions, which may lead to premature tool failure. To enhance tool performance during cutting, there is extensive application of coatings with high hardness, good wear resistance, and thermal stability onto high-speed steel (HSS) or WC-Co substrates (Ref 3-5). TiN, a first-generation hard coating, has been widely used in coated tools because of its high hardness and chemical stability (Ref 6, 7). However, TiN coatings are prone to oxidation at temperatures of 500-600 °C, limiting their application in high-temperature working conditions (Ref 8). An effective method to improve coating properties is to add a third element to TiN, forming a ternary coating (Ref 9, 10). For instance, TiCN coatings demonstrate better wear resistance (Ref 11, 12), thermal stability (Ref 13), and toughness (Ref 14) compared to TiN coatings. Traditional ceramics, such as Al_2O_3, have also been widely used as a coating material due to their favorable thermal properties, high chemical stability, and high hardness at high temperatures (Ref 15-17).

More recently, multilayered TiN/TiCN/Al_2O_3 coatings have been developed. For instance, Kuang et al. reported that the multilayered TiN/TiCN/Al_2O_3 coatings exhibited better oxidation resistance than individual coatings (Ref 18). Compared to single-layer coatings, a novel class of coatings with multilayered structures has demonstrated improved mechanical and tribological capabilities (Ref 19). Some researchers further treated the surface of multilayered coatings using shot-peening and observed an improvement in chipping resistance (Ref 20). They attributed this optimization to the increase in compressive stress on the coating surface and the refinement of the coating microstructure. For this reason, surface stress and microstructure control are employed as additional processing techniques in the preparation process.

High-current pulsed electron beam (HCPEB) technology has recently been demonstrated to be a potent tool for surface modification of many materials (Ref 21-23). During HCPEB irradiation, the outermost region experiences various physical processes, including rapid melting (10^7-10^8 K/s), evaporation, and solidification due to the high-density electron pulses ($\sim 10^4$ A/cm^2) of short duration (1.5 μs) (Ref 24). Meanwhile, HCPEB irradiation has a considerable "self-purification" effect on the sample surface, which corresponds to the eruption of impurities (Ref 25). Numerous studies have revealed that the substantial modifications induced by HCPEB irradiation might significantly enhance the mechanical properties of different coatings, particularly their hardness and wear resistance (Ref 26-28). Lou et al. investigated the effect of HCPEB irradiation on an as-deposited TiAlN coating, and the results showed that the bonding strength of the irradiated coating was effectively improved due to the elimination of residual tensile stress (Ref

Nana Tian, Fuyang Cao, Jintong Guan, and **Qingfeng Guan**, School of Materials Science and Engineering, Jiangsu University, Zhenjiang 212013, China; **Shiyu Zhou** and **Xiangming Chen**, Zhuzhou Cemented Carbide Cutting Tools Co., Ltd, Zhuzhou 412007, China; and **Conglin Zhang**, School of Material Science and Engineering, Yancheng Institute of Technology, Yancheng 221051, China. Contact e-mails: fuyangcao@ujs.edu.cn and guanqf@ujs.edu.cn.

29). Moreover, Anthony J. Perry found that HCPEB irradiation can eliminate defects, refine grain size, and reduce residual tensile stress of the TiN coating (Ref 7). However, limited research can be found regarding the influence of HCPEB irradiation on multilayered TiN/TiCN/Al_2O_3 coatings.

In this study, the effect of HCPEB irradiation pulses on the microstructure, roughness, residual stress, and mechanical properties of TiN/TiCN/Al_2O_3-coated carbide tools was investigated. Additionally, the tool wear and failure modes of the irradiated TiN/TiCN/Al_2O_3-coated carbide tools were analyzed in dry machining of 45# steel.

2. Experimental

2.1 Experimental Setup

(1) Preparation and HCPEB treatment of the multilayered TiN/TiCN/Al_2O_3 coatings

The multilayer TiN/TiCN/Al_2O_3 coatings were deposited using an automatic CVD system (Ionbond BPX Pro 530L). Substrates made of cemented carbide alloy (WC-Co(YG6)), comprising 94 wt.% WC and 6 wt.% Co, were employed. Before the application of coatings, all substrates were ground and polished to achieve a roughness of 0.2 μm. Subsequently, the substrates were cleaned by ultrasonic treatment in acetone for 30 minutes.

The formation of TiN layers is represented by the chemical reaction:

$$2TiCl_4(g) + N_2(g) + 4H_2(g) \overset{950^\circ C,200KPa}{\longrightarrow} 2TiN(s) + 8HCl(g) \quad \text{(Eq 2.1)}$$

The TiN deposition was carried out at a temperature of 950 °C and a pressure of 200 kPa. The gas ratio of $TiCl_4$ to N_2 was maintained at 1/30.

The formation of TiCN layers is represented by the chemical reaction:

$$TiCl_4(g) + 3/2H_2(g) + 1/3CH_3CN(g) \overset{885^\circ C,60KPa}{\longrightarrow} TiC_{2}/_{3}N_{1}/_{3}(s) + 4HCl(g) \quad \text{(Eq 2.2)}$$

TiCN deposition was performed at a temperature of 885 °C and a pressure of 60 kPa. The gas ratio of CH_3CN to $TiCl_4$ was set at 1/2, and the deposition time was 4 hours.

The following chemical reaction illustrates the formation of the Al_2O_3 layer:

$$2AlCl_3(g) + 3CO_2(g) + 3H_2(g) \overset{1000^\circ C,65KPa}{\longrightarrow} Al_2O_3(s) + 3CO(g) + 6HCl(g) \quad \text{(Eq 2.3)}$$

The deposition of the Al_2O_3 layer was conducted at a temperature of 1000 °C and a pressure of 65 kPa. The gas ratio for $AlCl_3$: CO_2: H_2S was maintained at 5:18:1.

Finally, TiN (~0.4 μm) + TiCN (~8 μm) + Al_2O_3 (~4 μm) multilayer coatings were deposited on the cemented carbide YG6 substrate.

(2) HCPEB treatment

The obtained multilayered coatings were irradiated using a "HOPE-I" type HCPEB system. The number of pulses was varied as 3, 5, 8, and 15. Table 1 presents the other key parameters for HCPEB irradiation. For more detailed information regarding the HCPEB irradiation conditions and processes, please refer to our previous research studies (Ref 30).

2.2 Microstructural Analysis

X-ray diffraction (XRD) using CuK_α radiation (= 0.154 nm) and operated at 37 kV and 40 mA with a Rigaku D/max-2500/pc instrument was used to identify the phase compositions of the multilayered coatings. The microstructural characteristics (grain morphology, cross-sectional topography and defects) of the coatings were comprehensively studied using a field emission scanning electron microscope (FE-SEM), specifically the FEI-nano 450 Model. Furthermore, the surface roughness was evaluated using a VK-X100/X200 three-dimensional laser scanning microscope (LSM).

2.3 Mechanical and Tribological Properties

The mechanical properties, including hardness and elastic modulus, were measured using a nano-indenter (Anton Paar TTX-NHT3) equipped with a Berkovich indenter. The load function consisted of 5 seconds of loading to 50 mN, followed by a 10-second hold, and then a 5-second unloading period. At least 10 indentation tests were carried out. In addition, the Oliver–Pharr method was used to calculate the modulus and hardness (Ref 31).

To measure the wear resistance of coatings in ambient air at room temperature, a ball-on-disk tribometer (MFT-4000, Lanzhou Huahui) was employed, in which a Si_3N_4 ball with a diameter of 4 mm served as the counter-body. The reciprocating wear tests were conducted with a sliding speed of 4 mm/s and a normal load of 5 N. The stroke length was set to be 5 mm. A whole run of the wear test lasted for 20 minutes. The wear rate (W) was calculated using Eq 1:

$$W = \frac{\Delta V}{LF} \quad \text{(Eq 1)}$$

where ΔV represents the measured wear volume, L is the sliding distance, and F is the applied normal load.

The cutting test was carried out on an HK80 type lathe, with the cutting speed (Vc), feed rate (fn), and cutting depth (ap) set to 300 m/min, 0.2 mm/r, and 1.0 mm, respectively. The flank wear on the inserts was measured every 5 minutes of cutting. Besides, the tool life was estimated according to the standard ISO 3685-1993, where a flank wear threshold of 0.3 mm was used as a criterion. The workpiece used in the cutting tests was 45# steel with a diameter of 200 mm and a length of 400 mm.

3. Results and Discussion

3.1 XRD Analysis

The XRD patterns of the multilayered coatings subjected to different number of irradiation pulses are depicted in Fig. 1. Figure 1(a) reveals that all coatings comprise phases of TiCN and Al_2O_3, with no new phases observed after irradiation. The absence of TiN diffraction peaks can be attributed to the total thickness of the outer Al_2O_3 and TiCN layers, which exceeds the penetration depth of x-rays. Notably, the gradual broadening of the Al_2O_3 (0 1 2) peaks can be attributed to the grain

Table 1 The HCPEB irradiation experimental parameters

Electron beam energy	Vacuum pressure	Energy density	Pulse time	Dwell time
27, kV	5.5 × 10^{-3}, Pa	4, J cm^{-2}	1.5, μs	15, s

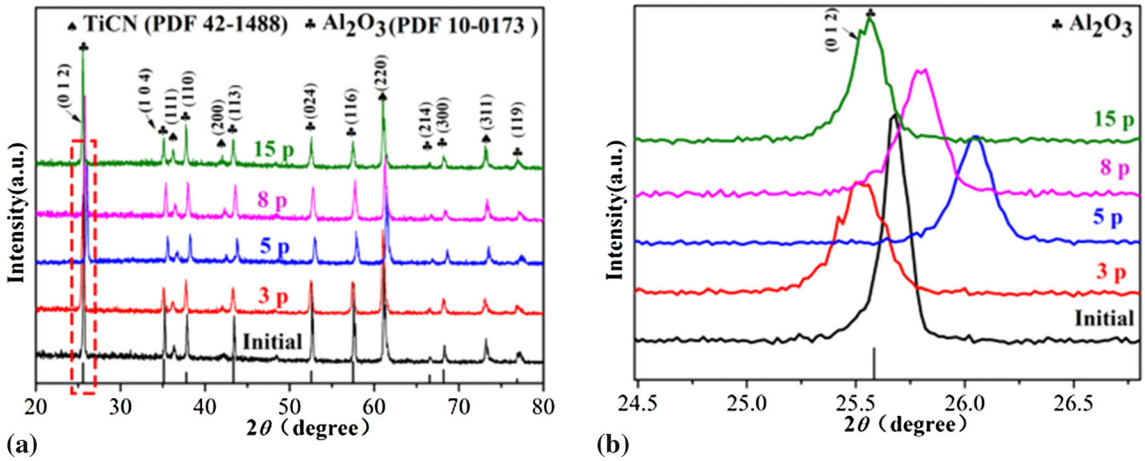

Fig. 1 XRD analysis of initial and irradiated TiN/TiCN/Al_2O_3-coated carbide tools surface. (a) XRD pattern; (b) enlarged image of the Al_2O_3 (012) diffraction peak

refinement and defects (e.g., dislocations) induced by HCPEB irradiation (Ref 32, 33). Previous studies have documented the formation of various defects, including dislocations and voids, on the surface of materials like Al (Ref 24) and GH4169 (Ref 32) following HCPEB treatment.

Figure 1(b) presents the magnified peaks of Al_2O_3 (0 1 2). The peak position of the initial, 5-, and 8-pulsed coatings shifts toward a higher angle compared to the standard PDF card (No. 10-0173). Such XRD peak shifting is generally associated with the presence of residual compressive stresses in the initial coating (Ref 34). In addition, the peak positions of Al_2O_3 (0 1 2) move to a lower angle after 3 and 15 pulses of irradiation, which suggests that residual tensile stress exists in the irradiated coatings. This observation is in agreement with previous research (Ref 35). More details about the stress generation process during HCPEB can be found in (Ref 36). In a previous study conducted by Anthony et al. (Ref 37), it was determined that coatings exhibiting a certain degree of compressive stress can enhance fatigue life, inhibit crack propagation, and improve resistance to stress corrosion of materials. Conversely, the presence of tensile residual stress reduces their performance capabilities.

3.2 Microstructure Characterization

Figure 2 illustrates the 3D morphology and surface roughness (Sa) of the initial and irradiated coatings. Figure 2(a) shows sharp protrusions and bulges on the surface of the initial coating, indicating its relatively rough nature. Following 3 pulses of irradiation, significant changes in 3D morphology can be observed, with most of the sharp protrusions and bulges eliminated by HCPEB irradiation. The subsequent images in Fig. 2(b-d) illustrate a clear transition from a rough surface in the initial coating to a flat surface in the 8-pulsed coating. The surface roughness (Sa) is calculated in Fig. 2(f), and the Sa for initial coating was found to be 0.213 μm. After 3, 5, 8, and 15 pulses of irradiation, the surface roughness was changed to 0.134, 0.127, 0.120 and 0.157 μm, respectively. As the number of irradiation pulses increased from 3 to 8, the roughness decreased significantly. This might be associated with the relatively gradual flattening of sharp protrusions and bulges (Ref 38). Furthermore, the "self-purification" effect induced by HCPEB irradiation might also be attributed to this observed phenomenon (Ref 39). Lou et al reported that a flattened coating surface positively affects reducing cutting forces and temperature at the tool-chip interface (Ref 29). However, the Sa value increased to 0.157 μm after 15 pulses. It is believed that the repetitive plastic deformation and the high strain rate experienced during multiple HCPEB pulses contribute to the increased roughness (Ref 40). After repeated pulses, microcracks and craters reappeared, ultimately leading to an increase in surface roughness.

Figure 3 shows the SEM morphology of the TiN/TiCN/Al_2O_3 coatings. Figure 3(a) reveals equiaxed grains with sizes ranging from 0.5 to 1 μm distributed on the initial coating surface, along with deposition defects such as holes and microcracks, that contribute to its highly rough appearance. SEM images of the TiN/TiCN/Al_2O_3 coatings after 3, 5, 8, and 15 HCPEB pulses are shown in Fig. 3(b-e), respectively. From Fig. 3(b), it can be seen that the density of microcracks on the coating surface increased, which might be attributed to the residual tensile stress in the coating (Ref 41, 42). In addition, numerous craters were formed at the crack boundaries, which

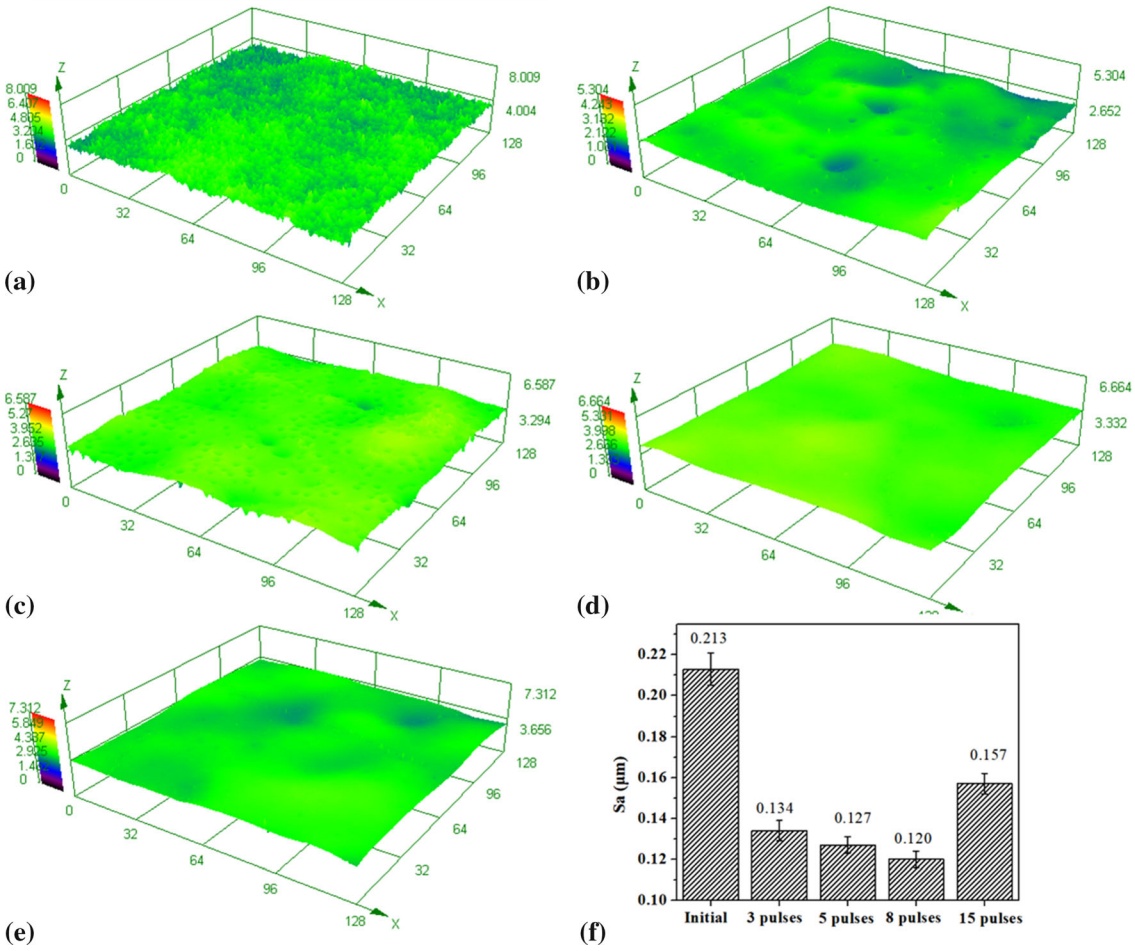

Fig. 2 The surface roughness of the TiN/TiCN/Al_2O_3 coatings after HCPEB irradiation (a) Initial; (b) 3 pulses; (c) 5 pulses; (d) 8 pulses; (e) 15 pulses; (f) the surface roughness of coatings

are typical manifestations resulting from localized sublayer melting and subsequent eruption through the outermost surface following HCPEB irradiation (Ref 43, 44). Additionally, the smoothest surfaces were observed in the coatings treated with 5 and 8 pulses of irradiation, as depicted in Fig. 3(c), (d). The variation in crater density corresponding to different numbers of HCPEB pulses is graphically represented in Fig. 3f. The observed trend of decreasing crater density with an increasing number of HCPEB pulses aligns with the findings reported in the literature (Ref 45), and the reduction in density can be attributed to the "self-purification" effect induced by HCPEB irradiation. Specifically, the craters formed on the coating surface after 3 pulses are subsequently fused or eliminated by the successive electron beam pulses, resulting in improved surface roughness. However, microcracks and craters reappear in the coatings irradiated with 15 pulses, as shown in Fig. 3e. According to Bilgin (Ref 46), the presence of such microcracks can be attributed to the deformation resulting from tensile stress caused by the disparity in thermal expansion coefficients between layers.

Figure 4 presents a schematic diagram illustrating the surface evolution and crack formation of the coating during HCPEB irradiation. Despite HCPEB irradiation being conducted in a vacuum (5.5×10^{-3} Pa), some residual gas inevitably remains in the microcracks or holes of the initial coating. When the electron beam contacts the residual gas, a plasma reaction occurs, resulting in the melting of the tip of Al_2O_3 equiaxed grains, which then fills into the valleys between grains (Ref 47). The plasma reaction and electrical breakdown effect of the gas cause the crack edge to rapidly rise to a high temperature under the condition of high current density (Ref 23, 48). The accumulated charge density at the crack increases with the increase in irradiation pulses, which will aggravate the electrical breakdown effect and finally lead to the melting of the crack edge. Repeated melting and filling during irradiation gradually flatten the coating surface.

Cross-sectional micrograph and EDS analysis of the TiN/TiCN/Al_2O_3 coating are present in Fig. 5. All coatings exhibit three layers: the upper Al_2O_3 layer, the subsurface TiCN layer, and the thin TiN transition layer. The initial coating shows

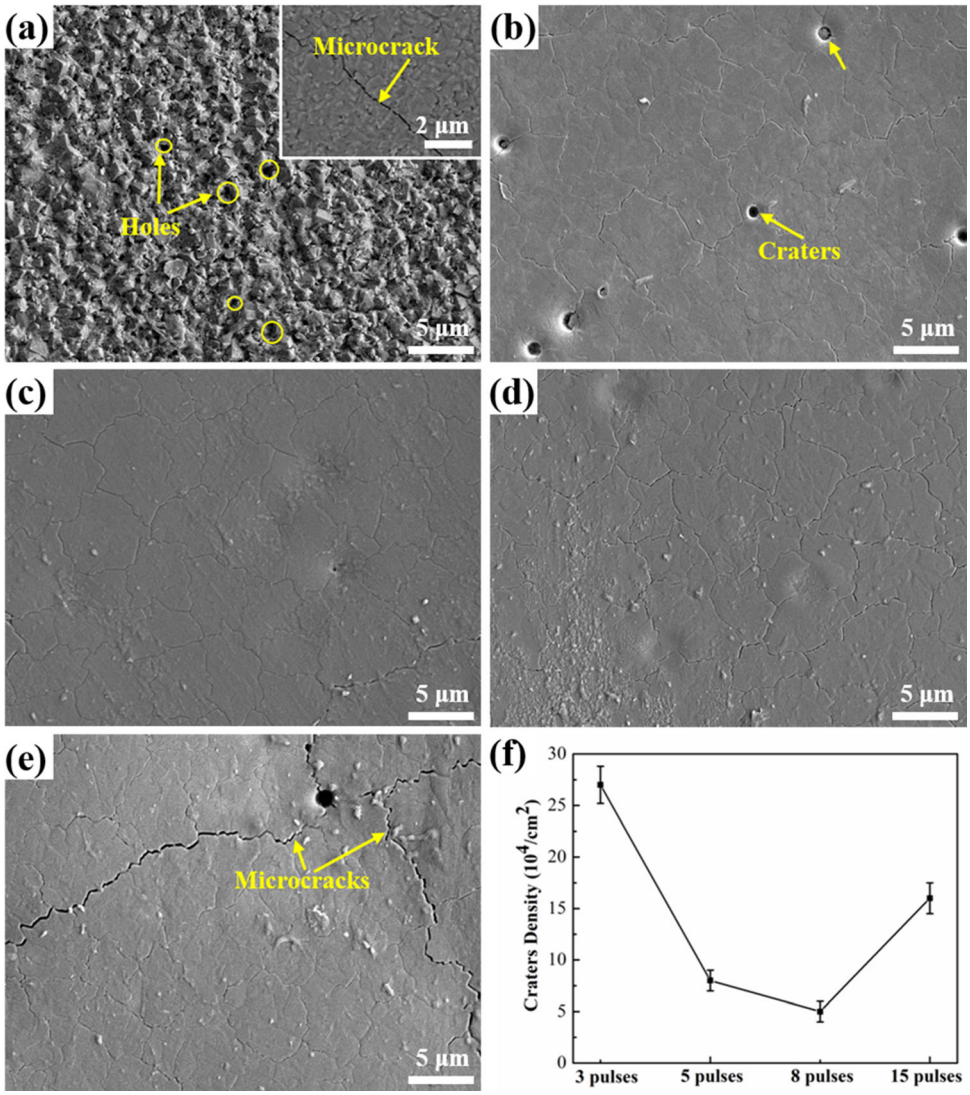

Fig. 3 SEM morphology of TiN/TiCN/Al_2O_3 coatings surface before and after HCPEB irradiation: (a) Initial; (b) 3 pulses; (c) 5 pulses; (d) 8 pulses; (e) 15 pulses; (f) the crater density of coatings

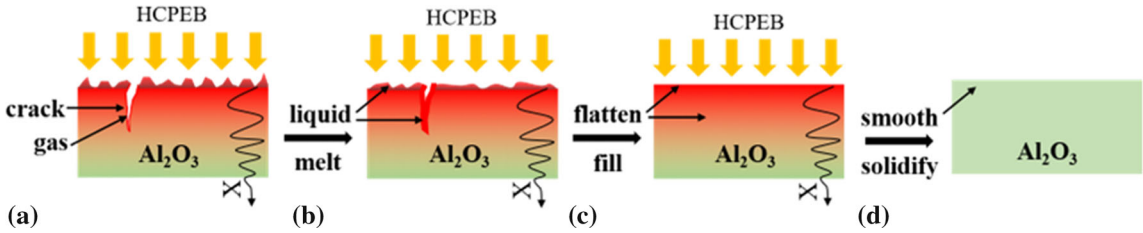

Fig. 4 Schematic diagram of sample surface melting

pores and lacks full density (Fig. 5a). In contrast, the 5-pulsed coating is fully densified due to the remelting effect of HCPEB. However, pores and cracks are observed in the 15-pulsed coating (Fig. 5c), attributed to the tensile stress caused by repeated thermal expansion mismatch between layers (Ref 7).

3.3 Mechanical Properties

The nano-indentation load–displacement curves (Fig. 6) show the deformation behavior of the initial, 5-pulsed, and 15-pulsed TiN/TiCN/Al_2O_3 coatings (Ref 49-51). Under a normal load of 50 mN, the penetration depth for the initial coating was approximately 0.353 μm. The 5-pulsed coating exhibited the minimum penetration depth, with a value of 0.328 μm, while the 15-pulsed coating showed a penetration depth of 0.352 μm. After unloading, there tends to be a residual offset in the displacement of all samples. According to the method proposed by Oliver et al. (Ref 31), the nano-hardness of the 5-pulsed coating exhibited the highest hardness by calculating the data from the load–displacement relationship.

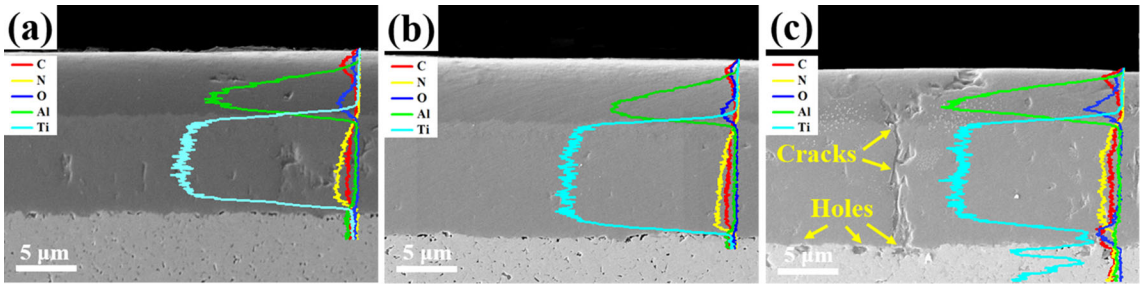

Fig. 5 The cross-sectional micrograph and EDS analysis: (a) initial; (b) 5-pulsed and (c) 15-pulsed TiN/TiCN/Al_2O_3 coating

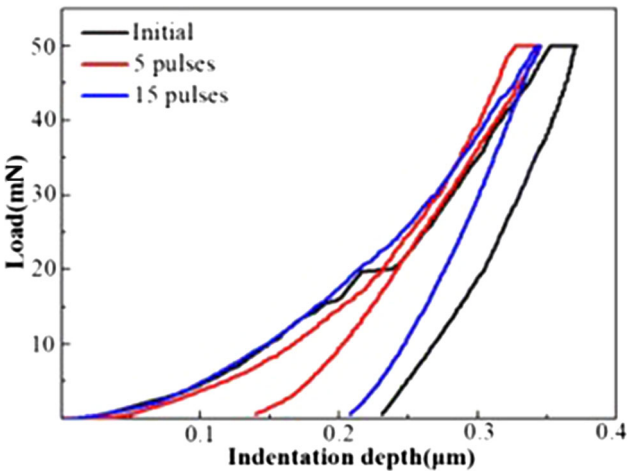

Fig. 6 Nanoindentation load–displacement curves for initial, 5-pulsed, and 15-pulsed TiN/TiCN/Al_2O_3 coatings

Figure 7 presents the mechanical properties of the initial and irradiated TiN/TiCN/Al_2O_3 coatings. The hardness slightly increased with increasing irradiation pulses, reaching a maximum for the 5-pulsed coating, followed by a slight decrease in hardness for the 8-pulsed and 15-pulsed coatings. The maximum hardness value obtained was 29.58 ± 1.1 GPa after 5-pulsed irradiation, surpassing values reported in previous works (Ref 15, 19). Several factors contributed to the hardening effect: the formation of abundant defects (dislocations and vacancies) on the coatings after HCPEB irradiation, hindering plastic deformations and leading to increased hardness (Ref 53); the reduction of holes and cracks on the coating surface after irradiation, positively influencing hardness (Ref 54); and the introduction of compressive residual stress, which also contributed to increased hardness, as suggested by Altenberger (Ref 55). Similar tendencies were observed in the elastic modulus values of these coatings.

The values of H/E and H^3/E^2 for the multilayered coatings are shown in Fig. 7(b). The wear resistance, which is associated with the ratio of plastic work to total work during indentation (Ref 56), correlates closely with the hardness-to-modulus ratio (H/E). Furthermore, H^3/E^2 represents the measure of resistance to plastic deformation (Ref 57). Coatings with higher values of H/E and H^3/E^2 generally exhibit favorable fracture toughness and resistance to plastic deformation. Based on all of these metrics, the 5-pulsed coated tool demonstrated the best wear resistance.

Figure 8 illustrates the friction coefficient (COF) curves and wear rates of both the initial and irradiated coatings. The initial coating exhibited a relatively high average friction coefficient of ~ 0.77 (Fig. 8a). In contrast, all treated coatings demonstrated lower friction coefficients than the initial coating. The 5-pulsed coatings showed a relatively stable friction coefficient with the lowest average value among all coatings. Figure 8(b) shows the average wear rates of the multilayer coatings, with the minimum wear rate (1.144×10^{-6} mm^3 N^{-1} m^{-1}) observed in the 5-pulsed coatings. The remarkable improvement in the tribological property of the 5-pulsed coatings can be attributed to the improvement in hardness, resistance to plastic deformation, and reduction in surface roughness. HCPEB irradiation effectively enhanced the friction and wear characteristics of the coatings, with the 5-pulsed coating demonstrating the most superior performance.

Figure 9 displays the progression of flank wear for both the initial and irradiated coated tools. All irradiated coatings exhibited significant improvement in wear resistance compared to the initial coating. Notably, the 5-pulsed coated tool demonstrated the longest cutting life, approximately 40 minutes, which is 33.3% higher than that of the initial coating tool. These results indicate that HCPEB treatment has a beneficial effect on improving tool life and wear resistance.

The rake and flank facets of the tools after cutting are shown in Fig. 10. The initial tool's blade exhibited chipping after 30 minutes of cutting (Fig. 10a), primarily due to the hard-brittle nature of the cemented carbide coating and stress concentration at the edge during high-speed cutting. The 3-pulsed irradiation tools showed accumulated built-up edges (BUEs) at the cutting edge after 30 minutes of cutting (Fig. 10b), a phenomenon attributed to the adhesion and growth of chips on the rake surface under the combined effect of high pressure and temperature during high-speed cutting (Ref 58). The 5- and 8-pulsed coated tools (Fig. 10c and d) exhibited only flank wear after cutting for 40 and 35 minutes, respectively. However, the 15-pulsed coated tools showed BUEs on the flank surface after 35 minutes of cutting (Fig. 10e), indicating that the porous service layer induced a decrease in the adhesion strength of coatings, as interpreted by K. Weigel (Ref 28).

Typically, the dominant wear mechanism is influenced by factors including the surface contact area, material properties, topography, and hardness (Ref 29). In this study, the improvement in tool wear performance resulted from the combination

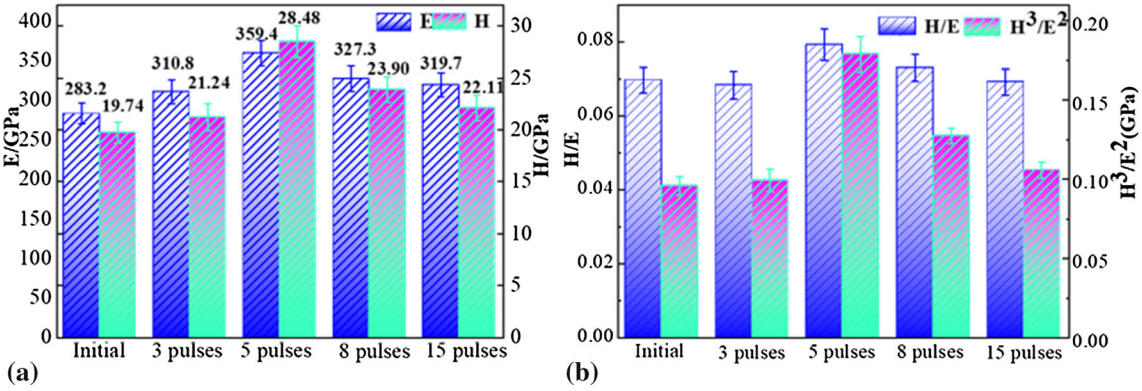

Fig. 7 Mechanical properties of the as-deposited TiN/TiCN/Al_2O_3 coatings: (a) Hardness and elastic modulus; (b) H/E and H^3/E^2

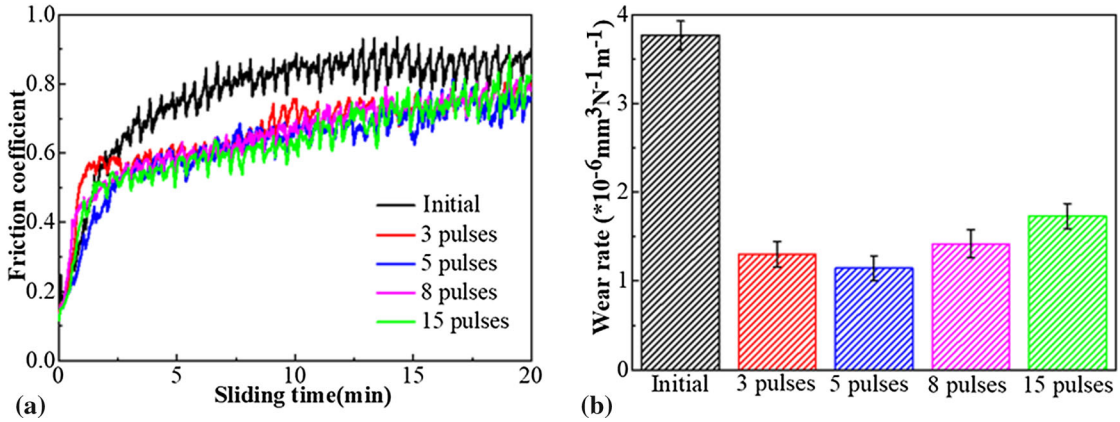

Fig. 8 Tribological behavior of the initial and HCPEB irradiated coatings: (a) Coefficient of friction and (b) wear rate

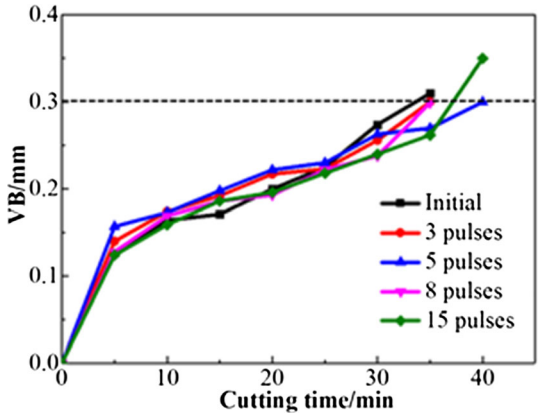

Fig. 9 Cutting life diagram of TiN/TiCN/Al2O3-coated carbide tools before and after HCPEB irradiation and VB curve diagram of flank wear

of roughness reduction, residual stress elimination, wear resistance improvement, and plastic reinforcement. The 5-pulsed irradiated coated tool demonstrated the most superior cutting performance, suggesting that an appropriate number of irradiation pulses effectively enhanced the surface quality.

4. Conclusions

This paper investigates the characteristics of a multilayer TiN/TiCN/Al_2O_3 coating deposited on carbide WC-Co through CVD, followed by treatment with HCPEB irradiation. Investigations on the characteristics of the treated coating and associated microhardness and wear behaviors were conducted. The main findings of the present work are as follows:

1) HCPEB irradiation results in broadened diffraction peaks due to grain refinement and defect formation. Additionally, the stress state of the coating surface changes, inducing compressive stress after 5 and 8 pulses of irradiation.
2) The irradiation process eliminates holes and grain valleys in the coating through the gas's plasma discharge and electric breakdown effect, leading to reduced surface roughness.
3) HCPEB irradiation significantly affects the nano-hardness (H) and elastic modulus (E) of the TiN/TiCN/Al_2O_3 coating. The values of H/E and H^3/E^2 initially increase and then decrease with increasing irradiation pulses, with the maximum values observed in the 5-pulsed coated tools.
4) Proper HCPEB irradiation pulses notably improve the friction and wear properties of TiN/TiCN/Al_2O_3-coated tools.

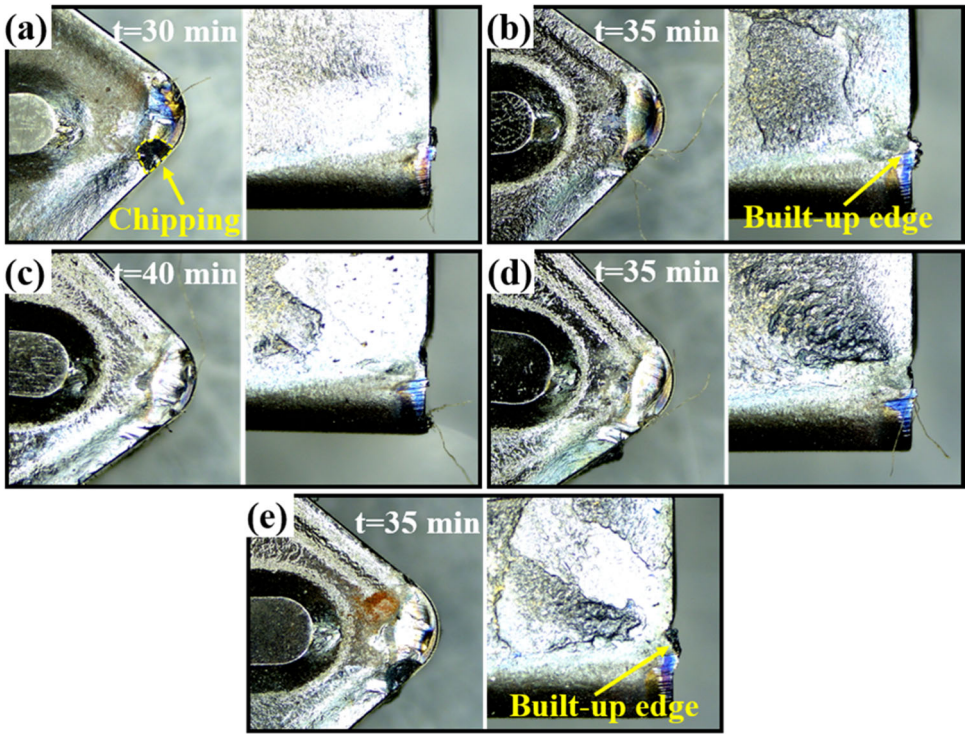

Fig. 10 The rake face and flank face of TiN/TiCN/Al2O3-coated carbide tools after the end of life: (a) Initial; (b) 3 pulses; (c) 5 pulses; (d) 8 pulses; (e) 15 pulses

5) HCPEB irradiation significantly enhances the cutting performance of coated tools. Coated tools subjected to 5 pulses exhibit a 33.3% increase in cutting life compared to the initial tool, with only flank wear observed as the failure mode.

Acknowledgments

This work was supported by the National Natural Science Foundation of China (NO.52001273) and the Natural Science Foundation of Jiangsu Province (BK20201062).

Author Contribution

NT was involved in validation, data analysis, and writing—original draft. SZ contributed to data analysis. CZ was involved in resources, supervision, and funding acquisition. FC contributed to methodology and conceptualization. JG and XC were involved in investigation and formal analysis. QG was involved in supervision, resources, and conceptualization.

Conflict of interest

The authors declare that they have no known competing financial interests or personal relationships that could have appeared to influence the work reported in this paper.

References

1. V. Sharma and P.M. Pandey, Recent Advances in Turning with Textured Cutting Tools: A Review, *J. Clean. Prod.*, 2016, **137**, p 701–715. https://doi.org/10.1016/j.jclepro.2016.07.138
2. H. Zhang, J. Xiong, Z. Guo, T. Yang, J. Liu, and T. Hua, Microstructure, Mechanical Properties, and Cutting Performances of WC-Co Cemented Carbides with Ru Additions, *Ceram. Int.*, 2021, **47**(18), p 26050–26062. https://doi.org/10.1016/j.ceramint.2021.06.011
3. B.D. Beake, L. Bergdoll, L. Isern, J.L. Endrino, G.S. Fox-Rabinovich, and S.C. Veldhuis, Influence of Probe Geometry in Micro-Scale Impact Testing of Nano-Multilayered TiAlCrN/NbN Coatings Deposited on WC-Co, *Int. J. Refract. Met. Hard Mater.*, 2020, **2021**(95), p 105441. https://doi.org/10.1016/j.ijrmhm.2020.105441
4. Z. Yuan, L. Liu, H. Song, Z. Lu, B. Yang, J. Xiong, N. Huang, and X. Jiang, Improvement in the Universality of High-Performance CVD Diamond Coatings on Different WC-Co Substrates by Introducing Multilayered Diamond/β-SiC Composite, *Diam. Relat. Mater.*, 2021, **116**, p 108369. https://doi.org/10.1016/j.diamond.2021.108369
5. J. Xiong, Z. Guo, M. Yang, S. Xiong, J. Chen, Y. Wu, B. Wen, and D. Cao, Effect of Ultra-Fine $TiC_{0.5}N_{0.5}$ on the Microstructure and Properties of Gradient Cemented Carbide, *J. Mater. Process. Technol.*, 2009, **209**(12–13), p 5293–5299.
6. M.T. Laugier, Adhesion of TiC and TiN Coatings Prepared by Chemical Vapour Deposition on WC-Co-Based Cemented Carbides, *J. Mater. Sci.*, 1986, **21**(7), p 2269–2272.
7. A.J. Perry, J.N. Matossian, S.J. Bull, D.I. Proskurovsky, P.C. Rice-Evans, T.F. Page, D.E. Geist, J. Taylor, J.J. Vajo, R.E. Doty, V. Rotshtein, and A.B. Markov, The Effect of Rapid Thermal Processing (RTP) on TiN Coatings Deposited by PVD and the Steel-Turning Performance of Coated Cemented Carbide, *Surf. Coatings Technol.*, 1999, **120–121**, p 337–342.
8. C. Kainz, N. Schalk, C. Saringer, and C. Czettl, In-Situ Investigation of the Oxidation Behavior of Powdered TiN, Ti(C, N) and TiC Coatings Grown by Chemical Vapor Deposition, *Surf. Coatings Technol.*, 2021, **406**, p 126633. https://doi.org/10.1016/j.surfcoat.2020.126633
9. A.A. Matei, I. Pencea, M. Branzei, D.E. Trancă, G. Ţepeş, C.E. Sfăt, E. Ciovica, A.I. Gherghilescu, and G.A. Stanciu, Corrosion Resistance Appraisal of TiN, TiCN and TiAlN Coatings Deposited by CAE-PVD

Method on WC-Co Cutting Tools Exposed to Artificial Sea Water, *Appl. Surf. Sci.*, 2015, **358**, p 572–578.
10. M. Simsir, Y. Palaci, and A. Özer, A Comparative Study of Hardness/Scratch/Wear Properties of TiCN and TiAlN Coatings on DIN 12842 Steel by CA-PVD Method, *J. Aust. Ceram. Soc.*, 2021, **57**, p 1–11.
11. P.C. Jindal, A.T. Santhanam, U. Schleinkofer, and A.F. Shuster, Performance of PVD TiN, TiCN, and TiAlN Coated Cemented Carbide Tools in Turning, *Int. J. Refract. Met. Hard Mater.*, 1999, **17**(1), p 163–170.
12. H. Cicek, Wear Behaviors of TiN/TiCN/DLC Composite Coatings in Different Environments, *Ceram. Int.*, 2018, **44**(5), p 4853–4858. https://doi.org/10.1016/j.ceramint.2017.12.074
13. K. Narasimhan, S.P. Boppana, and D.G. Bhat, Development of a Graded TiCN Coating for Cemented Carbide Cutting Tools-a Design Approach, *Wear*, 1995, **188**(1–2), p 123–129.
14. D. Landek, S. Jakovljević, V. Alar, and S. Kovačić, Effect of Steel Substrate on the Corrosion Properties of a Gradient Multilayer TiN/TiCN Coating Deposited by the PACVD Process, *Mater. Corros.*, 2019, **70**(2), p 307–318.
15. M. Fallqvist, M. Olsson, and S. Ruppi, Abrasive Wear of Texture-Controlled CVD α-Al_2O_3 Coatings, *Surf. Coatings Technol.*, 2007, **202**(4–7), p 837–843.
16. R. Connelly, A.K. Pattanaik, and V.K. Sarin, Development of Moderate Temperature CVD Al_2O_3 Coatings, *Int. J. Refract. Met. Hard Mater.*, 2005, **23**(4–6), p 317–321.
17. S. Ruppi, Deposition, Microstructure and Properties of Texture-Controlled CVD α-Al2O3 Coatings, *Int. J. Refract. Met. Hard Mater.*, 2005, **23**(4–6), p 306–316.
18. H. Kuang, D. Tan, W. He, Z. Yi, Z. Zou, and X. Wang, Oxidation Behavior of Multilayer Hard Coatings (TiCN/Al2O3/TiN) in Process of Recycling Coated Multicomponent Hardmetal Scrap, *Materials (Basel).*, 2018, **11**(10)
19. J. Liu, J. Xiong, L. Zhou, Z. Guo, H. Wen, Q. You, X. Li, J. Liu, and W. Zhao, Properties of TiN–Al2O3–TiCN–TiN, TiAlN, and DLC-Coated Ti(C, N)-Based Cermets and Their Wear Behaviors during Dry Cutting of 7075 Aluminum Alloys, *Int. J. Appl. Ceram. Technol.*, 2021, **18**(3), p 792–802.
20. A.B.H. Bejaxhin and G. Paulraj, *A Review on Effect of Coatings on Tools and Surface Roughness as Vibration Resistance*, 2017, **5**(10), p 50–57.
21. T. Grosdidier, J.X. Zou, N. Stein, C. Boulanger, S.Z. Hao, and C. Dong, Texture Modification, Grain Refinement and Improved Hardness/Corrosion Balance of a FeAl Alloy by Pulsed Electron Beam Surface Treatment in the "Heating Mode," *Scr. Mater.*, 2008, **58**(12), p 1058–1061.
22. Y. Hao, B. Gao, G.F. Tu, H. Cao, S.Z. Hao, and C. Dong, Surface Modification of Al-12.6Si Alloy by High Current Pulsed Electron Beam, *Appl. Surf. Sci.*, 2012, **258**(6), p 2052–2056.
23. C. Zhang, P. Lv, J. Cai, Y. Zhang, H. Xia, and Q. Guan, Enhanced Corrosion Property of W-Al Coatings Fabricated on Aluminum Using Surface Alloying under High-Current Pulsed Electron Beam, *J. Alloys Compd.*, 2017, **723**, p 258–265. https://doi.org/10.1016/j.jallcom.2017.06.189
24. N. Tian, S. Li, C. Zhang, J. Cai, P. Lyu, S. Konovalov, X. Chen, C.T. Peng, and Q. Guan, The Surface Modification of Aluminum by Mechanical Milling of Pb Coating and High Current Pulsed Electron Beam Irradiation, *Mater. Res. Express*, 2019, **6**(12), p 1265g3.
25. J. Cai, P. Lv, Q. Guan, X. Xu, J. Lu, Z. Wang, and Z. Han, Thermal Cycling Behavior of Thermal Barrier Coatings with MCrAlY Bond Coat Irradiated by High-Current Pulsed Electron Beam, *ACS Appl. Mater. Interfaces*, 2016, **8**(47), p 32541–32556.
26. Y. Hao, B. Gao, G.F. Tu, Z. Wang, and S.Z. Hao, Influence of High Current Pulsed Electron Beam (HCPEB) Treatment on Wear Resistance of Hypereutectic Al-17.5Si and Al-20Si Alloys, *Mater. Sci. Forum*, 2011, **675–677**, p 693–696.
27. V.P. Rotshtein, Y.F. Ivanov, A.B. Markov, D.I. Proskurovsky, K.V. Karlik, K.V. Oskomov, B.V. Uglov, A.K. Kuleshov, M.V. Novitskaya, S.N. Dub, Y. Pauleau, and I.A. Shulepov, Surface Alloying of Stainless Steel 316 with Copper Using Pulsed Electron-Beam Melting of Film-Substrate System, *Surf. Coatings Technol.*, 2006, **200**(22–23), p 6378–6383.
28. K. Weigel, K. Bewilogua, M. Keunecke, G. Bräuer, G. Grumbt, R. Zenker, and H. Biermann, Effects of Electron Beam Treatment on Ti(1–x)AlxN Coatings on Steel, *Vacuum*, 2014, **107**, p 141–144. https://doi.org/10.1016/j.vacuum.2014.04.023
29. C. Lou, L. Zhang, X. Lu, X. Lyu, G. Jin, and Q. Wang, Effects of High Current Pulsed Electron Beam Irradiation on the Mechanical Properties and Cutting Performance of TiAlN-Coated Tools, *J. Mater. Eng. Perform.*, 2017, **26**(12), p 5864–5870.
30. C. Zhang, P. Lv, J. Cai, C.T. Peng, Y. Jin, and Q. Guan, The Microstructure and Properties of Tungsten Alloying Layer on Copper by High-Current Pulse Electron Beam, *Appl. Surf. Sci.*, 2017, **422**, p 582–590. https://doi.org/10.1016/j.apsusc.2017.06.049
31. W.C. Oliver and G.M. Pharr, An Improved Technique for Determining Hardness and Elastic Modulus Using Load and Displacement Sensing Indentation Experiments, *J. Mater. Res.*, 1992, **7**(6), p 1564–1583. https://doi.org/10.1557/JMR.1992.1564
32. P. Lv, X. Sun, J. Cai, C. Zhang, X. Liu, and Q. Guan, Microstructure and High Temperature Oxidation Resistance of Nickel Based Alloy GH4169 Irradiated by High Current Pulsed Electron Beam, *Surf. Coatings Technol.*, 2017, **309**, p 401–409. https://doi.org/10.1016/j.surfcoat.2016.11.041
33. C. Zhang, P. Lv, H. Xia, Z. Yang, S. Konovalov, X. Chen, and Q. Guan, The Microstructure and Properties of Nanostructured Cr-Al Alloying Layer Fabricated by High-Current Pulsed Electron Beam, *Vacuum*, 2019, **167**, p 263–270. https://doi.org/10.1016/j.vacuum.2019.06.022
34. S. Zhang, H. Xie, X. Zeng, and P. Hing, Residual Stress Characterization of Diamond-like Carbon Coatings by an X-Ray Diffraction Method, *Surf. Coatings Technol.*, 1999, **122**(2–3), p 219–224.
35. K. Zhang, J. Ma, J. Zou, and Y. Liu, Surface Microstructure and Property Modifications in a Duplex Stainless Steel Induced by High Current Pulsed Electron Beam Treatments, *J. Alloys Compd.*, 2017, **707**, p 178–183. https://doi.org/10.1016/j.jallcom.2017.01.003
36. Q. Guan, Q. Zhang, and C. Dong, Physical Model of Stress and Deformation Microstructures in AISI 304L Austenitic Stainless Steel Induced by High-Current Pulsed Electron Beam Surface Irradiation, *ISIJ Int.*, 2008, **48**(2), p 235–239.
37. A.J. Perry, J.A. Sue, and P.J. Martin, Practical Measurement of the Residual Stress in Coatings, *Surf. Coatings Technol.*, 1996, **81**(1), p 17–28.
38. J. Cai, Q. Guan, X. Hou, Z. Wang, J. Su, and Z. Han, Isothermal Oxidation Behaviour of Thermal Barrier Coatings with CoCrAlY Bond Coat Irradiated by High-Current Pulsed Electron Beam, *Appl. Surf. Sci.*, 2014, **317**, p 360–369. https://doi.org/10.1016/j.apsusc.2014.08.049
39. Z. Zhang, S. Yang, P. Lv, Y. Li, X. Wang, X. Hou, and Q. Guan, The Microstructures and Corrosion Properties of Polycrystalline Copper Induced by High-Current Pulsed Electron Beam, *Appl. Surf. Sci.*, 2014, **294**, p 9–14. https://doi.org/10.1016/j.apsusc.2013.12.178
40. X. Lü, Y. Zhang, C. Lou, G. Li, and Q. Wang, Surface Modification of High Current Pulsed Electron Beam on Cemented Carbide Tools Using Response Surface Methodology, *Xiyou Jinshu/Chinese J. Rare Met.*, 2015, **39**(2), p 152–158.
41. J. Cai, Q. Guan, P. Lv, X. Hou, Z. Wang, and Z. Han, Surface Modification of CoCrAlY Coating by High-Current Pulsed Electron Beam Treatment under the "Evaporation" Mode, *Nucl. Instruments Methods Phys. Res. Sect. B Beam Interact. with Mater. Atoms*, 2014, **337**:90–96 https://doi.org/10.1016/j.nimb.2014.07.025
42. X. Mei, X. Liu, C. Wang, Y. Wang, and C. Dong, Improving Oxidation Resistance and Thermal Insulation of Thermal Barrier Coatings by Intense Pulsed Electron Beam Irradiation, *Appl. Surf. Sci.*, 2012, **263**, p 810–815.
43. D. Luo, G. Tang, X. Ma, L. Gu, M. Sun, and L. Wang, Various Categories of Defects after Surface Alloying Induced by High Current Pulsed Electron Beam Irradiation, *Appl. Surf. Sci.*, 2015, **351**, p 1069–1074.
44. Q.F. Guan, H. Zou, G.T. Zou, A.M. Wu, S.Z. Hao, J.X. Zou, Y. Qin, C. Dong, and Q.Y. Zhang, Surface Nanostructure and Amorphous State of a Low Carbon Steel Induced by High-Current Pulsed Electron Beam, *Surf. Coatings Technol.*, 2005, **196**(1–3), p 145–149.
45. S. Dong, C. Zhang, L. Zhang, J. Cai, P. Lv, Y. Jin, and Q. Guan, Microstructure and Properties of Cu-Cr Powder Metallurgical Alloy Induced by High-Current Pulsed Electron Beam, *J. Alloys Compd.*, 2018, **755**, p 251–256. https://doi.org/10.1016/j.jallcom.2018.04.291
46. S. Bilgin, O. Güler, Ü. Alver, F. Erdemir, M. Aslan, and A. Çanakçı, Effect of TiN, TiAlCN, AlCrN, and AlTiN Ceramic Coatings on

Corrosion Behavior of Tungsten Carbide Tool, *J. Aust. Ceram. Soc.*, 2021, **57**(1), p 263–273.
47. S. Guimond, U. Schütz, B. Hanselmann, E. Körner, and D. Hegemann, Influence of Gas Phase and Surface Reactions on Plasma Polymerization, *Surf. Coat. Technol.*, 2011, **205**(2), p S447–S450. https://doi.org/10.1016/j.surfcoat.2011.03.093
48. F.T.B. Macedo, M. Wiessner, C. Hollenstein, F. Kuster, and K. Wegener, Dependence of Crater Formation in Dry EDM on Electrical Breakdown Mechanism, *Procedia CIRP*, 2016, **42**, p 161–166. https://doi.org/10.1016/j.procir.2016.02.212
49. D. Ikeshima, K. Miyamoto, and A. Yonezu, Molecular Deformation Mechanism of Polycarbonate during Nano-Indentation: Molecular Dynamics Simulation and Experimentation, *Polymer (Guildf)*, 2019, **173**(April), p 80–87. https://doi.org/10.1016/j.polymer.2019.04.029
50. T.J. Marrow, I. Šulak, B.S. Li, M. Vukšić, M. Williamson, and D.E.J. Armstrong, High Temperature Spherical Nano-Indentation of Graphite Crystals, *Carbon N. Y.*, 2022, **191**, p 236–242.
51. D.Q. Doan, T.H. Fang, and T.H. Chen, Interfacial and Mechanical Characteristics of TiN/Al Composites under Nanoindentation, *Int. J. Solids Struct.*, 2021, **226–227**, p 111083. https://doi.org/10.1016/j.ijsolstr.2021.111083
52. T. Koyama, S. Uchida, and A. Nishiyama, Effect of Microstructure on Mechanical Properties and Cutting Performance of Al2O3-Ti(C, N) Ceramics, *Nippon Seramikkusu Kyokai Gakujutsu Ronbunshi/J. Ceram Soc. Jpn.*, 1992, **100**(1160), p 520–524.
53. G. Guo, G. Tang, X. Ma, M. Sun, and G.E. Ozur, Effect of High Current Pulsed Electron Beam Irradiation on Wear and Corrosion Resistance of Ti_6Al_4V, *Surf. Coat. Technol.*, 2013, **229**, p 140–145. https://doi.org/10.1016/j.surfcoat.2012.08.009
54. A.P. Ompusunggu, P. Sas, and H. Van Brussel, Distinguishing the Effects of Adhesive Wear and Thermal Degradation on the Tribological Characteristics of Paper-Based Friction Materials under Dry Environment: A Theoretical Study, *Tribol. Int.*, 2015, **84**, p 9–21. https://doi.org/10.1016/j.triboint.2014.11.016
55. M. Smaga, R. Skorupski, P. Mayer, B. Kirsch, J.C. Aurich, I. Raid, J. Seewig, J. Man, D. Eifler, and T. Beck, Influence of Surface Morphology on Fatigue Behavior of Metastable Austenitic Stainless Steel AISI 347 at Ambient Temperature and 300°C, *Procedia Struct. Integr.*, 2017, **5**, p 989–996.
56. A. Leyland and A. Matthews, On the Significance of the H/E Ratio in Wear Control: A Nanocomposite Coating Approach to Optimised Tribological Behaviour, *Wear*, 2000, **246**(1–2), p 1–11.
57. J. Musil, Hard and Superhard Nanocomposite Coatings, *Surf. Coatings Technol.*, 2000, **125**(1–3), p 322–330.
58. D. Cavaleiro, D. Figueiredo, C.W. Moura, A. Cavaleiro, S. Carvalho, and F. Fernandes, Machining Performance of TiSiN(Ag) Coated Tools during Dry Turning of $TiAl_6V_4$ Aerospace Alloy, *Ceram. Int.*, 2021, **47**(8), p 11799–11806.